Steel and Composite Structures, *Vol. 29, No. 6 (2018) 717-734*
DOI: https://doi.org/10.12989/scs.2018.29.6.717

Moment-rotation relationship of hollow-section beam-to-column steel joints with extended end-plates

Jia Wang [*1,2], Haiming Zhu [1a], Brian Uy [2b], Vipulkumar Patel [3c], Farhad Aslani [4,5d] and Dongxu Li [2e]

[1] *School of Civil and Environmental Engineering, The University of New South Wales, Sydney, NSW 2052, Australia*
[2] *School of Civil Engineering, The University of Sydney, Sydney, NSW 2006, Australia*
[3] *School of Engineering and Mathematical Sciences, College of Science, Health and Engineering, La Trobe University, PO Box 199, Bendigo, VIC 3552, Australia*
[4] *School of Civil Environmental and Mining Engineering, The University of Western Australia, Crawley, WA 6009, Australia*
[5] *School of Engineering, Edith Cowan University, WA 6027, Australia*

(*Received August 16, 2018, Revised December 2, 2018, Accepted December 23, 2018*)

Abstract. This paper presents the flexural performance of steel beam-to-column joints composed of hollow structural section beams and columns. A finite element (FE) model was developed incorporating geometrical and material nonlinearities to evaluate the behaviour of joints subjected to bending moments. The numerical outcomes were validated with experimental results and compared with EN1993-1-8. The demountability of the structure was discussed based on the tested specimen. A parametric analysis was carried out to investigate the effects of steel yield strength, end-plate thickness, beam thickness, column wall thickness, bolt diameter, number of bolts and location. Consequently, an analytical model was derived based on the component method to predict the moment-rotation relationships for the sub-assemblies with extended end-plates. The accuracy of the proposed model was calibrated by the experimental and numerical results. It is found that the FE model is fairly reliable to predict the initial stiffness and moment capacity of the joints, while EN1993-1-8 overestimates the initial stiffness extensively. The beam-to-column joints are shown to be demountable and reusable with a moment up to 53% of the ultimate moment capacity. The end-plate thickness and column wall thickness have a significant influence on the joint behaviour, and the layout of double bolt-rows in tension is recommended for joints with extended end-plates. The derived analytical model is capable of predicting the moment-rotation relationship of the structure.

Keywords: hollow section; beam-to-column joint; moment-rotation relationship; demountability; component method

1. Introduction

Beam-to-column steel joints have been employed in frames for decades due to their advantages in processing, manufacturing, transportation, construction and disposal at the end of a building's life. The most common structural form consists of I-section beams, stiffened or unstiffened H-shaped cross-section columns, end-plates and bolts shown in Fig. 1(a). In addition, the hollow structural section (HSS) columns shown in Fig. 1(b) are favoured as an alternative to the columns mentioned above due to the high performance (Han *et al*. 2008, Thai *et al*. 2017). Concrete is allowed to be filled into the HSS columns, thereby increasing the moment capacity. However, local buckling is inevitable to occur in beam webs or beam flanges adjacent to the joints under hogging moments, which leads to a capacity reduction. EN1993-1-8 (2005) presents various types of hollow section connections, one of which is a T joint or X joint with both hollow section members being welded together. Compared with I-section beams, hollow-section beams exhibit high flexural rigidity and rotational capacity. Therefore, they are preferred for application in seismic resistant buildings. From a research point of view, an investigation into the behaviour of beam-to-column joints with hollow section members shown in Fig. 1(c) is warranted.

EN1993-1-8 (2005) (EC3) provides common structural design guidance for traditional beam-to-column joints. Three main structural properties, including the moment resistance, rotational stiffness and rotation capacity, are defined to assess the moment-rotation (M-ϕ) relationship. An integral procedure is established to determine the structural properties by using the component method (CM). It is noted that the method has been applied in previous research. Augusto *et al*. (2016a) and (2016b) carried out a series of tests to investigate the behaviour of double-extended end-plate partial-strength beam-to-column joints. Based on the experimental tests, finite element (FE) models were developed to predict the moment-rotation relationship of the joints. The experimental and numerical results demonstrated that out-of-plane deformations occurred in H-shaped columns. Grimsmo *et al*. (2015) conducted tests to

*Corresponding author, Ph.D.,
E-mail: jia.wang@sydney.edu.au
[a] B.Eng., E-mail: haimingzhu1993@gmail.com
[b] Professor, E-mail: brian.uy@sydney.edu.au
[c] Lecturer, E-mail: v.patel@latrobe.edu.au
[d] Senior Lecturer, E-mail: farhad.aslani@uwa.edu.au
[e] Ph.D., E-mail: dongxu.li@sydney.edu.au

ISSN: 1229-9367 (Print), 1598-6233 (Online)

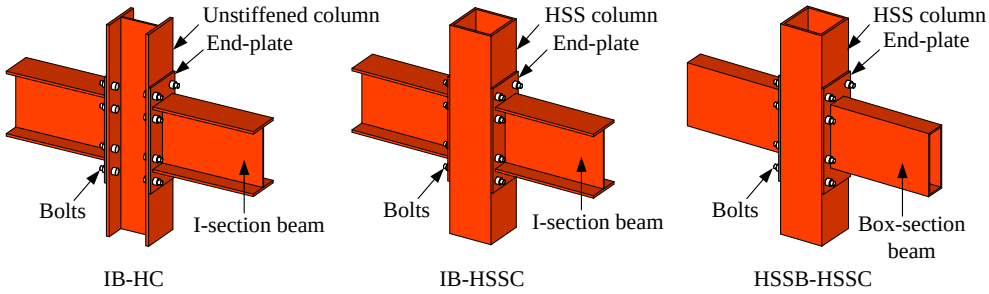

Fig. 1 Bolted joints with different component types

Table 1 Tests of steel beam-to-column joints with extended end-plates

Reference	Joint type	Joint ID	Beam					Column					End-plate			Bolt
			L_b (mm)	D_b (mm)	B_{bf} (mm)	t_{bf} (mm)	t_{bw} (mm)	H_c (mm)	D_c (mm)	B_{fc} (mm)	t_{fc} (mm)	t_{wc} (mm)	H_{ep} (mm)	B_{ep} (mm)	t_{ep} (mm)	d_b (mm)
Grimsmo *et al.* (2015)	IB-HC	QS-DLD-4	850	171	180	9.5	6	831	220	220	16	9.5	246	220	12	16
Augusto *et al.* (2016a)	IB-HC	J1.1	1147	360	170	12.7	8	3000	310	300	15.5	9	540	220	18	24
	IB-HC	J3.1	1147	360	170	12.7	8	3000	320	300	20.5	11.5	540	220	18	24
	IB-HC	J4.1	1147	270	280	13	8	3000	310	300	15.5	9	450	300	18	24
Coelho *et al.* (2004)	IB-HC	FS1	1200	300	150	10.7	7.1	1200	377	309	40	21	400	150	10	20
	IB-HC	FS2	1200	300	150	10.7	7.1	1200	377	309	40	21	400	150	15	20
	IB-HC	FS3	1200	300	150	10.7	7.1	1200	377	309	40	21	400	150	20	20
	IB-HC	FS4	1200	300	150	10.7	7.1	1200	377	309	40	21	400	150	10	20
Coelho and Bijlaard (2007)	IB-HC	EEP_15_2	1300	310	300	15.5	9	1540	340	310	39	21	435	300	15	24
	IB-HC	EEP_10_2a	1300	310	300	15.5	9	1540	340	310	39	21	435	300	10	24
	IB-HC	EEP_10_2b	1300	310	300	15.5	9	1540	340	310	39	21	435	300	10	24
Korol *et al.* (1993)	IB-HSSC	S3	2272	349	127	8.5	5.8	1200	203	203	12.7	12.7	520	170	19	20
	IB-HSSC	S4	2201	349	127	8.5	5.8	1200	254	254	9.53	9.53	550	230	19	20
	IB-HSSC	S5	2198	349	127	8.5	5.8	1200	254	254	11.13	11.13	590	230	22	20
Author	HSSB-HSSC	-	1500	250	150	9	9	1000	300	300	12.5	12.5	500	300	12	16

evaluate the behaviour of double-sided bolted beam-to-column joints subjected to severe impulsive loads. All tested specimens achieved bearing capacities where bolt fracture along with significant plastic deformations of end-plates was observed. Conclusions were made that the joints possessed satisfactory properties under the extreme loads. Coelho *et al.* (2004) and Coelho and Bijlaard (2007) performed tests on the beam-to-column joints at large deflections. Tests revealed that an increase in the thickness of end-plates resulted in an increase in the initial stiffness and flexural capacity but a decrease in the rotation capacity. Meanwhile, sufficient ductility was achieved by using high strength steel which retained high yield ratios and limited deformation capacities. Some other characteristics such as stiffness, fire resistance and cyclic behaviour were considered in relevant literature (Qiang *et al.* 2014, Sun *et al.* 2015, Odrobiňák *et al.* 2014, Petrina 2016, Nogueiro *et al.* 2009, da Silva *et al.* 2004).

It is noted that the research mentioned above were all limited to the structural form with H-shaped columns. With respect to HSS columns, Korol *et al.* (1993) and Ghobarah *et al.* (1996) performed experimental and numerical analysis for blind bolted joints. Blind fasteners were introduced which had been commonly utilised through continuous evolutions and improvements. Although the procedure determining the stiffness and capacity of the joints was similar with Eurocodes, its formulation had changed a lot due to the variation in the cross-section of columns. France *et al.* (1999) tested I-section beam-to-tubular column joints involving various parameters that influenced the rotational stiffness and moment capacity. The test outcomes denoted that certain key parameters controlled the design of the joints.

The corresponding configuration details of tested prototypes are collected and summarised in Table 1, in which only sub-assemblages with extended end-plates and two bolt-rows in tension are considered. The specimens are categorised into three types including I-section beam-to-H shaped column joints (IB-HC), I-section beam-to-hollow structural section column joints (IB-HSSC) and hollow structural section beam-to-hollow structural section column joints (HSSB-HSSC). It can be seen that most literature

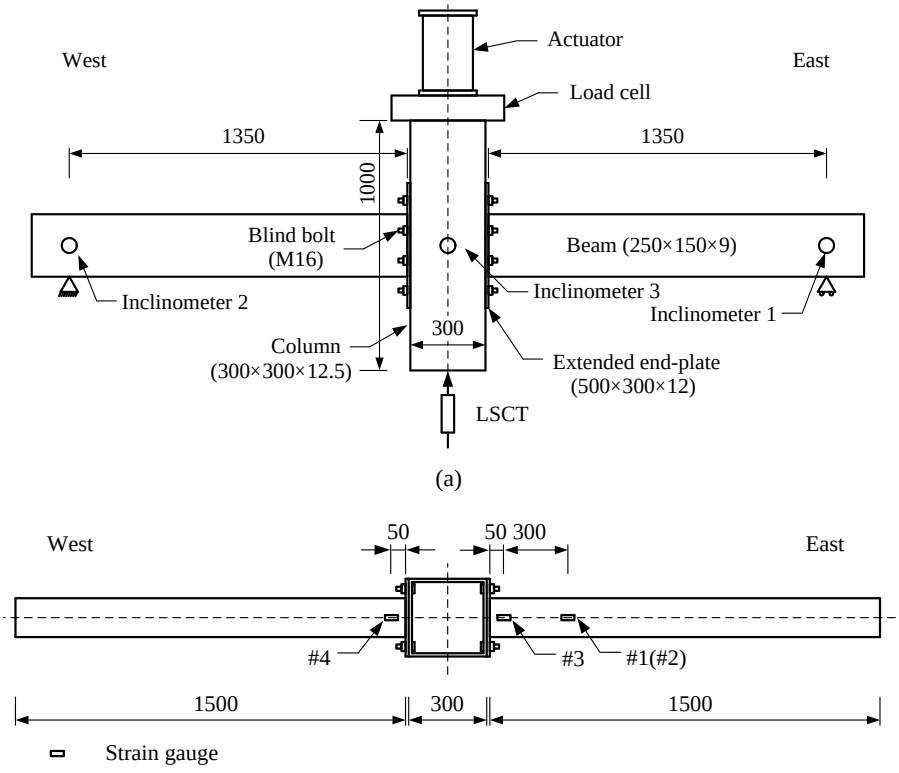

Fig. 2 Test specimen and loading arrangement (Units: mm)

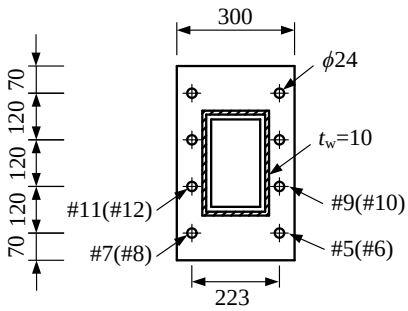

Fig. 3 End-plate geometry (Units: mm)

focused on the behaviour of the joints with I-section beams. There is a lack of research on joints incorporating hollow structural section beams. Therefore, the moment-rotation relationship of the joints consisting of HSS beams, HSS columns, extended end-plates and blind bolts needs to be investigated via experiments.

Moreover, the concept of reducing carbon footprint has been proposed and has become a significant discussion point in construction practice. In Australia, approximately 40% of landfill waste comes from the building and construction field (Uy *et al.* 2017), and the fact is building construction is responsible for almost a quarter of Australian greenhouse emissions. Therefore, some measurements, such as reusing and recycling of steel materials, have to be introduced to address this issue. Accordingly, an alternative approach is to develop demountable structures (Wang *et al.* 2018b, Li *et al.* 2016a, b, Rehman *et al.* 2016), which aims to allow the demolition procedure to be made much easier and faster, thereby lowering energy consumption and saving time as well as workload in a scientific and environmentally-sound manner. This paper intends to introduce the concept of demountability prompting a broad application of demountable structures.

This paper is organised into five main parts. Experimental performance of HSS beam-to-HSS column joints is initially investigated, and numerical analysis is then

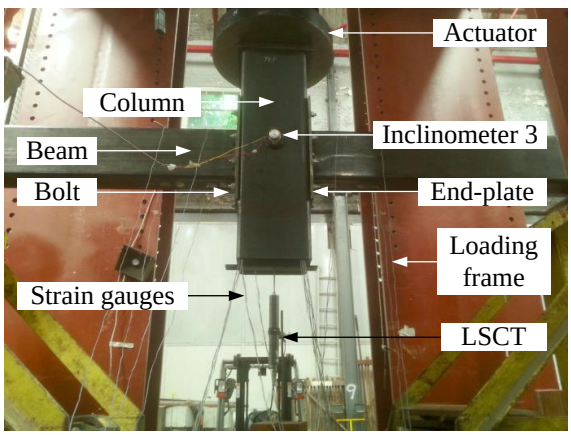

Fig. 4 Test set-up

Table 2 Geometry and property details of steel components

Component	Section size (mm)	f_y (MPa)	f_u (MPa)	E (GPa)	Pretension (kN)
HSS column	300×300×12.5	309	580	210	-
Beam	250×150×9	321	560	209	-
End-plate	500×300×12	312	591	218	-
Blind bolt	M16	640	800	200	59

employed to evaluate specific moment resisting behaviour. After highlighting the demountability of the structures, an analytical method is utilised to predict the initial stiffness and moment resistance with the aim of recommending design specifications for this structural form.

2. Experimental programme

2.1 Test details and instrumentation

As shown in Fig. 2, two hollow section beams were welded to the extended end-plates before attaching to the surface of an HSS column. Blind bolts were utilised to fix the end-plates against the column providing a convenient assembly and easy access from the external wall of the tube. Table 2 summarises the relevant details of each component. A section profile for the column was 300 mm × 300 mm × 12.5 mm which is commonly used in practice, and the beam was a 250 mm × 150 mm × 9 mm hollow steel tube. 12 mm thick end-plates with pre-drilled holes were welded to the HSS beams before being delivered to the laboratory at the University of New South Wales. These configurations are depicted in Fig. 3.

Strain gauges, inclinometers and Linear Strain Conversion Transducer (LSCT) were utilised to record strain data, rotations and translations respectively shown in Fig. 2. Four strain gauges were located on beam flanges for tracing the strain development, and eight gauges were set to the blind bolts adjacent to end-plates in tension. In order to investigate the strain distribution of the bolts, these gauges were mounted near the bolt heads with the shanks filed down to a reduced diameter to provide flat surfaces. This reduction is too small to have a significant effect on the failure mode of the bolts. Small holes were drilled through the heads to pass through the cables that were used to record strain data from the gauges. Two inclinometers were attached to beams 150 mm away from the ends to record beam rotations. Inclinometer 3 located on the central line of the column was taken as a controlled one to monitor if the loading condition was symmetrical. Deflections caused by the actuator were obtained via the LSCT installed underneath the column as shown in Fig. 2(a).

The set-up for the specimen is illustrated in Fig. 4. Due to geometrical symmetry, the specimen can be upside down to achieve the hogging moment for the joint. Both ends of the beams were simply supported which allowed for in-plane rotations.

2.2 Loading protocol

The specimen was subjected to monotonic loading by using a 5000 kN hydraulic actuator. The test was carried out under displacement control with a constant speed of 0.1 mm/min. Before the formal loading, all blind bolts were tightened to a torque of 190 N·m referred to the recommendation of the bolt manual. The purpose is to assure the column and the end-plates have been attached firmly to generate friction as well as resistance. A trial loading was implemented first to check if all instrumentation sensors worked functionally. Accordingly, the specimen was initially loaded up to 10 kN and unloaded if all sensors worked well, and then the specimen was reloaded up to failure. The failure was judged by monitoring the strain data of the bolts. When the strain value approached 0.02, the test was terminated since higher strains might induce sudden fracture and subsequent unpredictable risks in the lab.

2.3 Material properties

Coupon strength tests for the structural steel material were performed in accordance with AS 1391 (2007). Table 2 presents details of the material properties. Observation of the blind bolt showed no apparent yielding in terms of the stress-strain curve. The nominal yield stress accounting for 80% of the ultimate stress was hence recommended by AS 1252 (2016) and AS 4100 (1998). Similarly, its Young's Modulus can be obtained based on 40% of the yield stress and the corresponding strain.

2.4 Experimental results

Results including the moment-rotation (M-ϕ) relationship were extracted from the experimental test, and the data were compared with EC3 which were presented in Fig. 5 and Table 3. The behaviour of the flexural joint was typically reflected by the M-ϕ curve that described the relationship between the applied bending moment and the corresponding rotation. For the tested specimen, the bending moment (M) corresponded to the applied load (P) multiplied by the distance between the loading point and the surface of the end-plate attached to the column (L_{load})

$$M = PL_{load} \tag{1}$$

Chord rotation (ϕ), which corresponded to deflections of beams divided by beam length, was adopted to denote the joint rotation. It is acceptable since the flexural deformations of HSS beams can be ignored. Two options were used to describe ϕ experimentally, namely data from the inclinometer located on the beam web or readings from the LSCT mounted underneath the column. Since free vertical constraints were applied to the column, deformations of the column flange adjacent to the central line of the end-plate were accounted in the same manner as the point where the LSCT was placed. Therefore rotations resulting from end-plate deformations can be herein described by the LSCT which is taken as

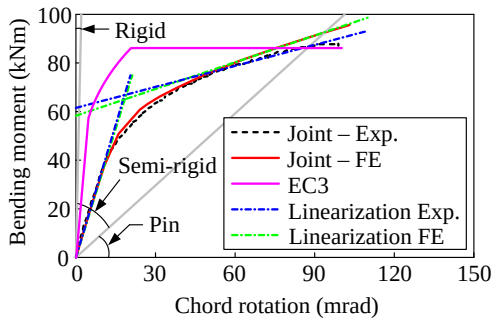

Fig. 5 M-ϕ curves for specimen

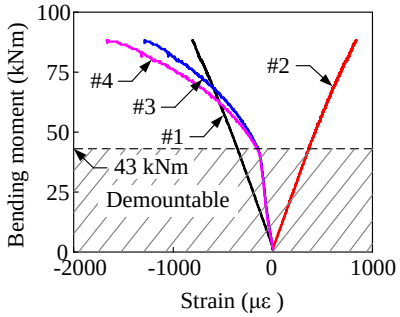

Fig. 6 Moment-strain responses for beams

$$\varphi = \arctan\left(\delta_{\mathrm{LSCT}} / L_{\mathrm{load}}\right) \tag{2}$$

The flexural curve can be categorised into three stages, which consisted of the elastic stage, plastic stage and strain-hardening stage. The elastic stage was characterised by initial rotational stiffness ($S_{\mathrm{j,ini}}$) which was identified by a secant line between the original point and $M_{\mathrm{j,E}}$ in the coordinate system. For the strain-hardening stage, the relevant stiffness ($S_{\mathrm{j,pl}}$) was defined by establishing a linearised slope based on the M-ϕ curves. It was quite divergent in various conditions and can only be established on a case-by-case basis.

In accordance with EC3, if initial stiffness for unbraced frames lies between 0.5 $EI_{\mathrm{b}}/L_{\mathrm{b}}$ and $k_{\mathrm{b}}EI_{\mathrm{b}}/L_{\mathrm{b}}$, a joint should be classified as a semi-rigid connection, namely

$$S_{\mathrm{j,ini}} \geq 0.5EI_{\mathrm{b}} / L_{\mathrm{b}}, \text{ and } S_{\mathrm{j,ini}} \leq k_{\mathrm{b}}EI_{\mathrm{b}} / L_{\mathrm{b}} \tag{3}$$

where k_{b} is taken as 25 for unbracing frames.

As shown in Fig. 5, the steel beam-to-column joint can be regarded as a semi-rigid connection, which conformed to the general rule for bolted connections. In a comparison between the test and EC3, it is worth noting that there existed significant divergences, especially in terms of the initial stiffness. The initial stiffness obtained from EC3 was approximately two times larger than that from the experiment. This may be attributed to the fact that the analytical model in EC3 was based on joints with I-section beams and H-shaped columns. Due to the location of column webs, flexural deformations of end-plates can be reduced at the very beginning, which resulted in a higher rotational stiffness. It demonstrated that EC3 was not adequately qualified to offer design guidance for joints with HSS beams and HSS columns. It directly led to a considerable overestimation of the initial stiffness. On the other hand, it is observed that EC3 was capable of predicting the moment capacity reasonably well. In accordance with the standard, the moment capacity was governed by the failure of the end-plate in bending. Therefore, shapes of columns or beams rarely affected the moment capacity ($M_{\mathrm{j,R}}$).

2.4.1 Beam in tension and compression

Fig. 6 depicts moment-strain responses of the beam subjected to tension and compression. #1 and #2 described the behaviour of beam flanges on the top and the bottom respectively. It can be seen that their absolute values of initial stiffness were similar and the behaviour kept elastic. It demonstrated that the neutral axis of the beam lay in the geometrical centre of the beam web. With respect to #3 and #4 which were strain gauges on two sides of beam flanges closed to the end-plate, the moment-strain curves exhibited the elastic-plastic performance. It is noted that the stiffness in the plastic stages deviated from each other. The deviation may be due to the non-uniform deformations of the beams resulting from an assembly error.

2.4.2 End-plate in bending and bolts in tension

Fig. 7 illustrates deflections of the end-plate in bending, which was typical for an equivalent T-stub model in tension. Meanwhile, the critical deformations agreed with the prediction of the moment capacity in EC3 where the capacity was dominated by the end-plate in bending. For the tested specimen, deformations of the end-plate were restrained by the bolts adjacent to the plate tip, and a slip between the end-plate and the column was not observed.

Fig. 7 Failure modes in experimental and numerical model

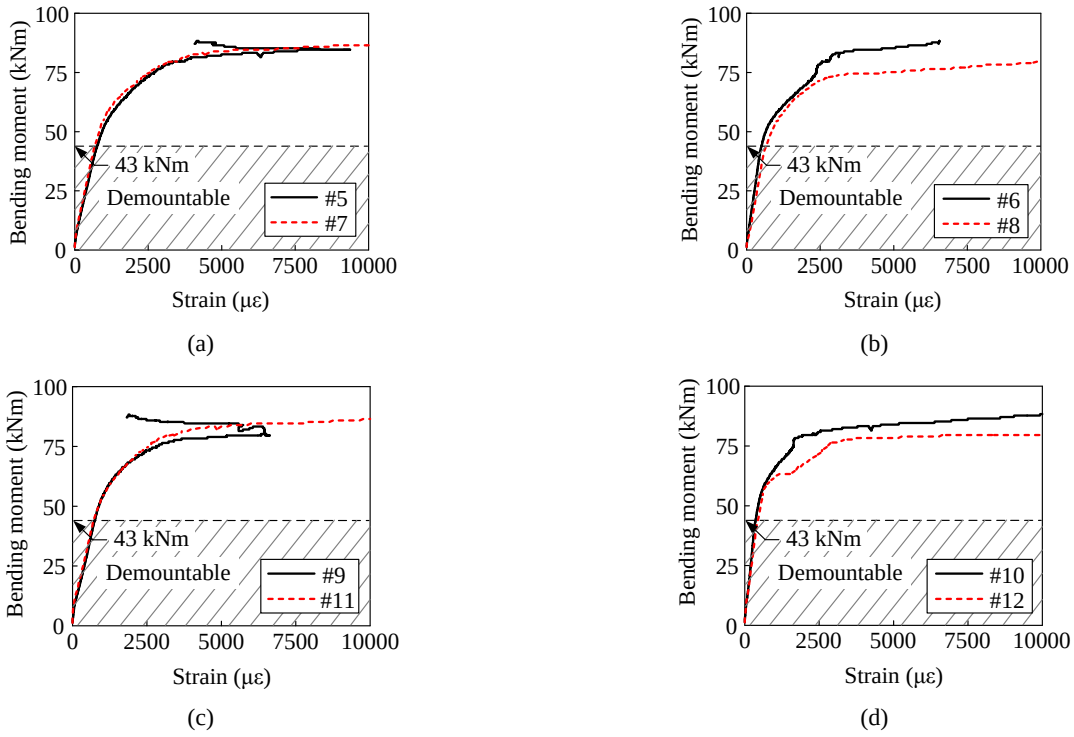

Fig. 8 Moment-strain responses for blind bolts

Therefore, the bolts were mainly subjected to tension. A fact should be pointed out that the tension of the bolts discussed in this paper referred to that resulting from deformations of the end-plate rather than pretension of bolts. Fig. 8 shows the experimental moment-strain responses of bolts in tension. All bolts achieved plastic behaviour resulting in large elongations. As mentioned in Section 2.2, loading was stopped when the bolt strain approached 0.02. In order to give a detailed description of the elastic properties, the strain was hence limited to 0.01 in the diagrams. The vast majority of the strain data were reliable to reflect the performance of bolts in tension. It is noted that the strain #5 and #9 appeared to decrease along with an increase in the bending moment. It is probably due to strain gauge damage

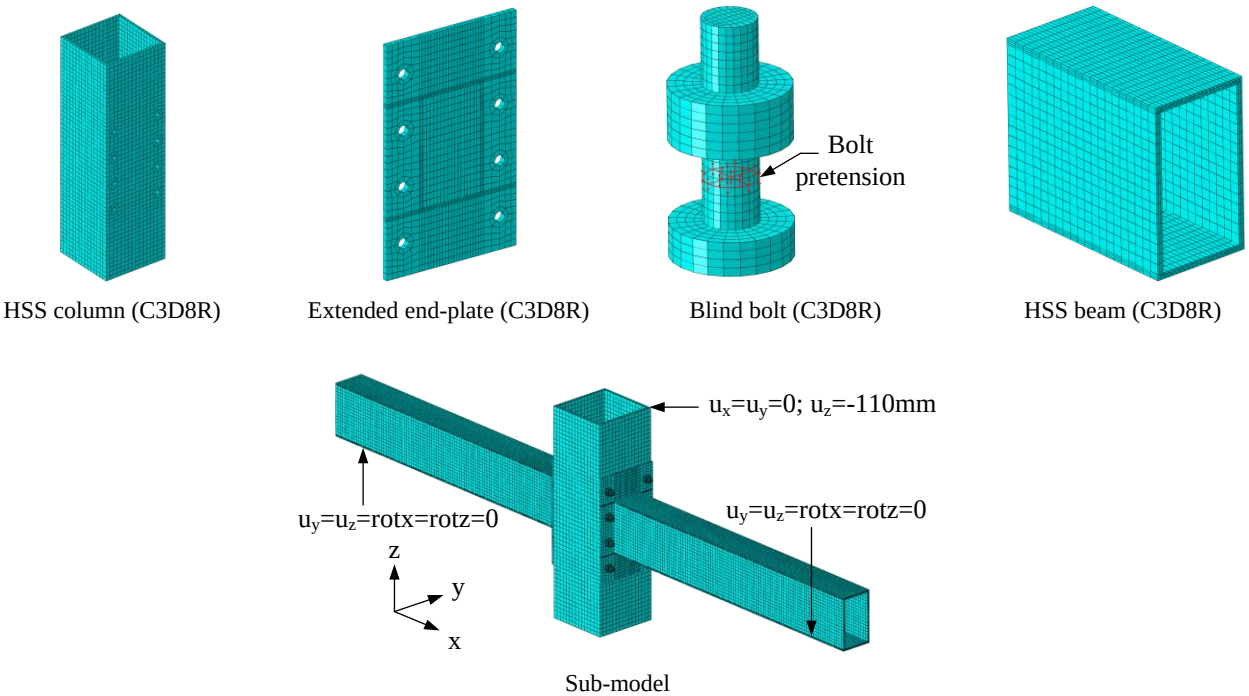

Fig. 9 Mesh parts of finite element model

as the bolt shanks may touch the inner surfaces of bolt holes on the end-plates or the columns.

Overall, the plastic behaviour of the end-plate imposed a significant influence on the moment capacity of the whole joint. Moreover, deflections of the end-plate caused large elongations of bolts in tension.

2.4.3 Feasibility analysis of demountability

The beam-to-column joint was designed with the aim of being dismantled for reuse and recycling of the steel materials at the end of its service life. Technically, the key point is to evaluate if all components of the structure remain elastic when reaching the maximum elastic bending moment ($M_{j,E}$). Once the assumption is valid, the structural form is viewed to be demountable. Even though there are slight residual deformations which occur on the structure after being unloaded or dismantled, the small deformations hardly obstruct the reuse and recycling so that they can be ignored.

It is clear to observe in Fig. 6 that the beam remained elastic before the applied moment rose up to around 43 kN·m. Meanwhile, there was no plastic strain which occurred on the blind bolts at the load within the shaded region as indicated in Fig. 8. Therefore, the results demonstrated that it was feasible to achieve demountability for the steel beam-to-column joints. Overall, the load capacity in terms of demountability accounted for about 53% of the ultimate strength. It was larger than the typical service load that is usually assumed to be about 40% of the ultimate load. Accordingly, when the frame reached the serviceability limit state in practice, the steel components were capable of being dismantled and reused directly without extra reprocessing.

3. Numerical modelling

3.1 Finite element model

A three-dimensional nonlinear FE model was developed by using the Abaqus software (2014). As shown in Fig. 9, all subassemblies including the HSS beams, HSS column, extended end-plates and blind bolts were taken into consideration. Due to the complex nonlinear analysis like large deformations and contact interactions, these components were modelled with three-dimensional solid elements. The available FE models were eight-node linear brick elements with reduced integration (C3D8R). They were capable of providing more realistic and accurate FE analysis results as well as reducing the computation time. In case of stress concentration around the blind bolts, a finer mesh size was adopted to eliminate stress variations (Mirza and Uy 2011). It is important to note that reduced integration elements possibly reduce the stiffness when it comes to structures governed by flexural deformations. This effect can impose a negative influence on the accuracy of the results in turn. To avoid the issue, at least three layers of elements were taken into account across the beam thickness.

The pretension of bolts was simulated via bolt load and length adjusting options available in the software. Second-order effects were included throughout the analysis to consider large deformations. The FE analysis was composed of two steps involving different boundary conditions and loading protocols. In the first step, the beams were simply supported at both ends. The column and the blind bolts were fixed temporarily in case of the motion of free bodies. Meanwhile, a low level of pretension was applied to all bolts to ensure that the contact interaction had been established. In the second step, the temporary constraints for the column and blind bolts were removed, and the bolt pretension was increased to the value that was mentioned above. Simultaneously, the vertical loading was applied on top of the column through displacement control up to 110 mm.

Stress-strain relationships for steel components are similar, namely exhibiting an elastic response followed by the yielding and strain-hardening behaviour. For the steel beams, HSS column and end-plates, trilinear models were adopted referred to the experimental and numerical studies conducted by Loh *et al*. (2006). For the blind bolts, the stress-strain relationship was simulated with a bilinear model due to its improved capacity to reflect the behaviour of the high strength structural steel.

An appropriate definition of contacted surfaces between the components is important for the FE model since it can influence the accuracy of results and convergence of the programme. Accordingly, a surface-to-surface contact in the model was employed by defining the penalty formulation for the tangential behaviour and the hard contact for the normal behaviour. The coefficient in the penalty friction formulation was set as 0.1 which was applied to all contact interactions. In the tested specimen, the end-plates were welded to the beams, and thus a tie constraint was adopted for the FE model.

3.2 Validation of numerical model

In this section, a detailed analysis of the joint was performed. The numerical results are also presented in Fig. 5 and Table 3. It is clear to see that numerical analysis had good agreement with the experimental outcomes. Fig. 5 shows that the FE model can not only provide a correct prediction for elastic responses but also exhibits high accuracy in the plastic behaviour. Data in Table 3 denote that although there were small distinctions between the experimental and FE results in terms of the moment $M_{j,E}$ and the initial stiffness ($S_{j,ini}$), the FE model predicted the moment capacity reasonably well. Fig. 7 illustrates similar deformations of the numerical model and tested specimen. Experimentally, 26 mm deflections occurred in the end-plate that was subjected to bending moments, which was also reflected by the FE model.

3.3 Parametric studies

The FE method, which had been proven to be reliable, was used to conduct a parametric study and the varied parameters are outlined in Table 4. In total, six parameters were taken into account for investigating the effect on the moment-rotation response of the steel beam-to-column joints.

Table 3 Main properties of moment-rotation curves for joints

	Resistance (kNm)		Stiffness (kNm/rad)			Chord rotation (mrad)	
	$M_{j,E}$	$M_{j,R}$	$S_{j,ini}$	$S_{j,pl}$	$S_{j,pl}$/ $S_{j,ini}$ (%)	$\phi_{Mj,E}$	$\phi_{Mj,R}$
Joint – Exp.	46	88	3648	289	8	14	99
Joint – FE	43	≥96	3527	367	10	13	≥103
EC3	58	86	12478	0	0	5	≥100
$\frac{\text{(Joint - FE)-(Joint - Exp.)}}{\text{Joint - Exp.}}$ (%)	-7	≥9	-3	27	-	-7	≥4
$\frac{\text{(EC3)-(Joint - Exp.)}}{\text{Joint - Exp.}}$ (%)	26	-2	242	-100	-	-64	1

Table 4 Parametric study on steel beam-to-column joints

Parameter	Configuration			
Steel yield strength, f_y (MPa)	300	340	360	
End-plate thickness, t_{ep} (mm)	8	10	12	16
Beam thickness, t_b (mm)	6	9	12.5	
Column wall thickness, t_c (mm)	12.5	16		
Blind bolt diameter, d_b(mm)	16	20	24	
Bolt-row in tension	Single		Double	

3.3.1 Effect of steel yield strength (f_y)

Fig. 10(a) describes the behaviour of steel beam-to-column joints with a variation in yield strength. For consistency purposes, the altered yield strength was applied to all steel components except for the blind bolts. In the meantime, since the steel yield strength was taken to investigate the effect of steel properties on the structural response, it was not necessary to select specific steel profiles. In this case, three types of yield strength were adopted for a simple analysis. Table 6 summarises the relevant numerical results that reflect the key characteristics of structures. It is observed that an increase in yield strength resulted in an enhanced plastic performance directly. Nonetheless, it is noted that the elastic behaviour which can be presented by the initial stiffness was approximately similar. The phenomenon was to be expected as the yield strength hardly affected the elastic response which was theoretically governed by the elastic modulus. In this case, the variable of steel yield strength was not able to benefit the demountability. Although the high yield strength improved the moment capacity of the steel beam-to-column joints, the construction cost may be increased as well. As a result, a conclusion can be drawn that reasonable and economical steel yield strengths should be selected for design guidance.

3.3.2 Effect of end-plate thickness (t_{ep})

In accordance with the design guidance, an end-plate is a critical component that influences the initial stiffness and the moment capacity. Since its moment of inertia is related to thickness cubed, the thickness is taken into consideration for comparison rather than its width or height.

The comparison of numerical results with the thickness ranging from 8 mm to 16 mm is depicted in Fig. 10(b). It can be seen that an increase in the end-plate thickness enhanced the initial stiffness and the plastic behaviour significantly. In particular, the initial stiffness of the joint with 16mm thick end-plates was about twice as that with 8 mm thick end-plates. It can also be found that the strain-hardening stiffness had a slight change, namely $S_{j,ini}$-to-$S_{j,pl}$ ratio rose from 8% to 12%. This is due to the fact that the strain-hardening stiffness only had a certain correlation with the initial stiffness. Based on the observation, it is concluded that an increase in the joint behaviour can be achieved by increasing the end-plate thickness. Accordingly, two options are favoured. The first one is to directly increase the thickness, while the second is to add one more plate between the end-plate and the column.

3.3.3 Effect of beam thickness (t_b)

The design of joints in EC3 specified a solution on the initial stiffness and moment capacity for the joints with I-section beams and H-shaped cross-section columns. In accordance with the design code, only the beam web in tension may contribute to the moment resistance. Moreover, as discussed in Section 2.4.1, an effect of the beam web in tension can be ignored, which led to no direct relationships between the beam thickness and the joint performance. However, the issue that whether the design rules are applicable for the joints with HSS beams and HSS columns or not remains uncertain. The parametric analysis of the beam thickness was hence carried out.

It can be seen in Fig. 10(c), a discrepancy in the plastic behaviour occurred to some extent, and there were small distinctions in the elastic behaviour as well. It is proved that contribution from the beams to the joint behaviour should not be neglected which was opposite to EC3. It is also found that increasing the beam thickness from 6 mm to 12.5 mm led to an increase in the moment resistance only by 8%. Therefore, strengthening the performance of the joint may not mainly depend on an increase in the beam thickness.

3.3.4 Effect of column wall thickness (t_c)

Fig. 10(d) depicts the results with different column wall thicknesses varying from 12.5 mm to 16 mm. The HSS columns were utilised instead of the H-shaped columns that were specified in the EC3. It is found that there existed large distinctions where the thick column improved the joint

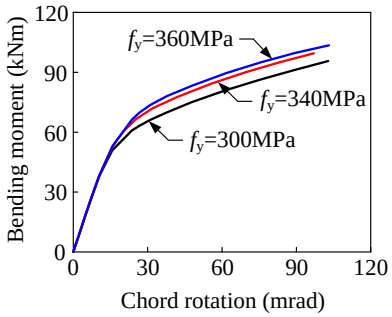

(a) Effect of steel yield strength

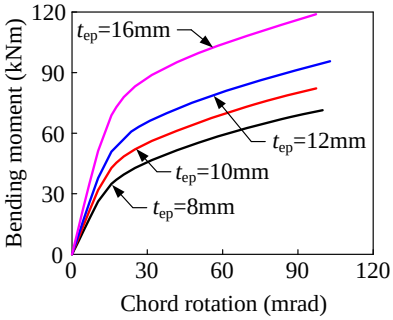

(b) Effect of end-plate thickness

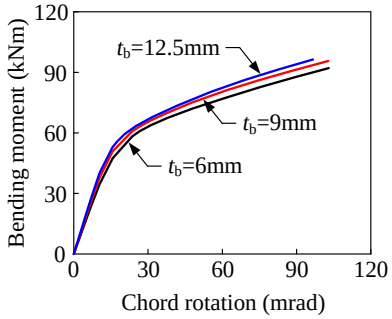

(c) Effect of beam thickness

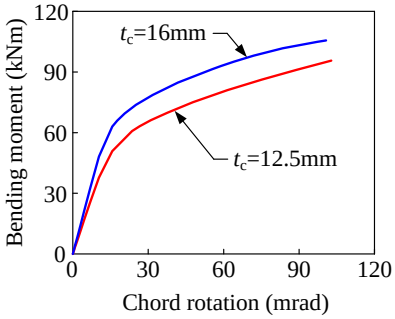

(d) Effect of column wall thickness

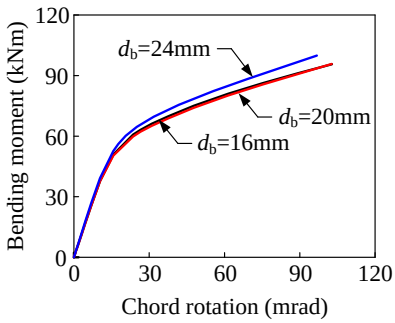

(e) Effect of bolt diameter

Fig. 10 Parametric analysis results

behaviour significantly. Similar to the effect of the end-plate thickness, it is because the performance of the structure benefitted from the column flange attached to the end-plate. A thicker column flange guaranteed a higher rigidity, thereby leading to a higher moment resistance. As a result, in terms of the demountability, thick columns were recommended in preference to assure the structural reliability.

3.3.5 Effect of bolt diameter (d_b)

Generally, the failure mode of steel beam-to-column joints included the fracture of blind bolts in tension and end-plates in bending. An assumption was that an increase in the bolt diameter might contribute to a higher moment capacity. Common bolt configurations applied in practice were M16, M20 or M24. Therefore, the effect of these three types of bolts was discussed.

It is worth to note from Fig. 10(e) that the joints with M16 and M20 blind bolts exhibited almost the same performance. However, the numerical results of M24 blind bolts deviated from the others after approaching the plastic behaviour. The deviation may be attributed to the assumption mentioned above. On the whole, the improvement did not appear to be evident, and M16 or M20 blind bolts were thus normally recommended.

3.3.6 Effect of number of bolts and bolt location

The number and layout of blind bolts assembled to end-plates were capable of influencing the joint behaviour, especially for the blind bolts in tension. To reflect a real-life scenario, a comprehensive situation needed to be accounted. Based on the literature review and engineering practice, the layout of bolts was divided into two sections, namely single bolt-row in tension and double bolt-rows in tension. Also, the controlled model, which possessed identical configurations with the tested specimen, was named with SBRT-0 and DBRT-0 respectively for comparison.

Effect of single bolt-row in tension

Fig. 11(a) shows four bisymmetric layout types of single bolt-row in tension. The geometric arrangement for SBRT-1 was very commonly applied in the bolted flush end-plate

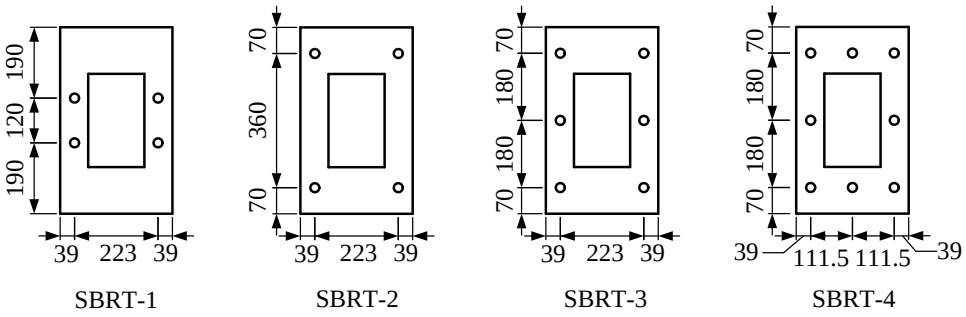

(a) Single bolt-row in tension

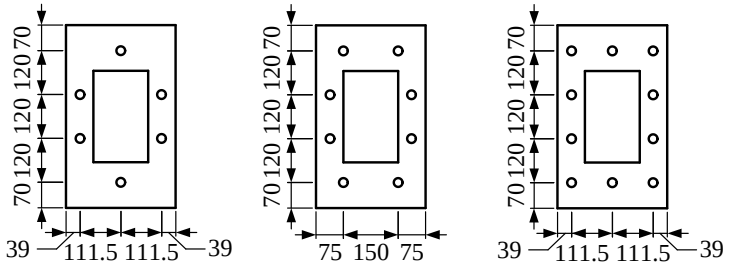

(b) Double bolt-rows in tension

Fig. 11 Layout of blind bolts on end-plate (Unit: mm)

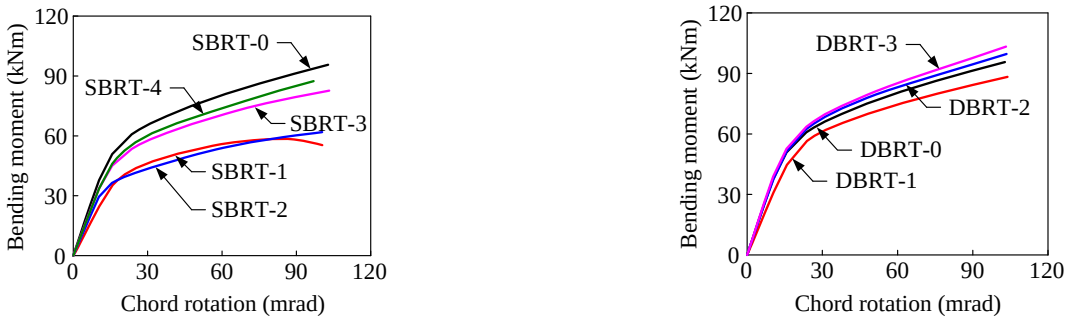

(a) Single bolt-row in tension

(b) Double bolt-rows in tension

Fig. 12 Effect of number of bolts and bolt location

joints, while the set-up for SBRT-2 merely takes four bolts into account in the extended region of the end-plate. Besides, more bolts were added to SBRT-3 and SBRT-4.

Fig. 12(a) illustrates the specific moment-rotation relationships of these models. It can be seen that the performance of joints with single bolt-row in tension was weaker than those with double bolt-rows in tension. It demonstrated that the layout with double bolt-rows in tension was more reasonable and practical for the joints with extended end-plates. By comparing SBRT-1 with SBRT-2, although both possessed similar behaviours, SBRT-1 reached the moment capacity much earlier than SBRT-2 due to bolt failure. By comparing SBRT-2 and SBRT-3, the performance can be increased significantly by adding bolts around the neutral axis. This is due to the fact that the moment lever arm for SBRT-3 was reduced by the additional bolts, leading to an increase in the stiffness and moment capacity. In addition, adding more bolts in tension like SBRT-4 was capable of benefiting the structural behaviour to a certain extent, but the benefit still cannot win the joint with double bolt-rows in tension. Overall, it was not recommended to set up single bolt-row in tension for the extended end-plates in terms of the demountability.

Effect of double bolt-rows in tension

As discussed above, double bolt-rows in tension were favoured for the extended end-plates. Fig. 11(b) indicates three forms of the layout which changed the number of the farthest bolts in tension from one to three.

It is observed in Fig. 12(b) that more bolts in the far end achieved higher stiffness as well as higher moment resistance, even though the increment was less evident than the effect caused by the end-plate thickness or the column wall thickness. Besides, a difference between DBRT-0 and DBRT-2 was that a relative space of bolts in the far end was changed. A highlight finding was that narrowing bolts in the far end was able to improve the structural behaviour to some extent. However, since the improvement achieved was

Table 5 Comparison of moment resistance and stiffness between experiments and EC3

Reference	Joint type	Joint ID	$M_{j,pc}$(exp) (kNm)	$M_{j,pc}$(EC3) (kNm)	$M_{j,pc}$(exp)/ $M_{j,pc}$(EC3)	$S_{j,ini}$(exp) (kNm/rad)	$S_{j,ini}$(EC3) (kNm/rad)	$S_{j,ini}$(exp)/ $S_{j,ini}$(EC3)
Grimsmo *et al.* (2015)	IB-HC	QS-DLD-4	150.8	140.8	1.07	13070	13392	0.98
Augusto *et al.* (2016a)	IB-HC	J1.1	335.0	355.0	0.94	71340	60246	1.18
	IB-HC	J3.1	395.0	389.0	1.02	95057	72950	1.30
	IB-HC	J4.1	304.0	271.0	1.12	38495	37865	1.02
Coelho *et al.* (2004)	IB-HC	FS1	107.5	77.5	1.39	17515	34660	0.51
	IB-HC	FS2	167.9	132.1	1.27	22695	46760	0.49
	IB-HC	FS3	182.5	187.3	0.97	22395	51760	0.43
	IB-HC	FS4	164.6	124.4	1.32	16665	32770	0.51
Coelho and Bijlaard (2007)	IB-HC	EEP_15_2	245.0	369.0	0.66	35300	58000	0.61
	IB-HC	EEP_10_2a	173.0	184.0	0.94	17200	31900	0.54
	IB-HC	EEP_10_2b	188.0	184.0	1.02	19900	34300	0.58
Korol *et al.* (1993)	IB-HSSC	S3	130.0	169.5	0.77	45470	48977	0.93
	IB-HSSC	S4	136.0	150.7	0.90	14500	30969	0.47
	IB-HSSC	S5	161.0	165.8	0.97	20370	41717	0.49
Author	HSSB-HSSC	-	61.5	86.0	0.72	3648	12478	0.28

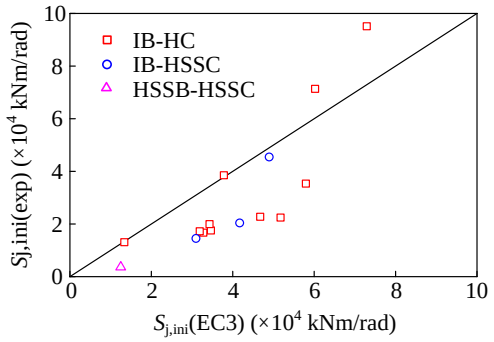

Fig. 13 Comparison of initial stiffness obtained from experiments and EC3

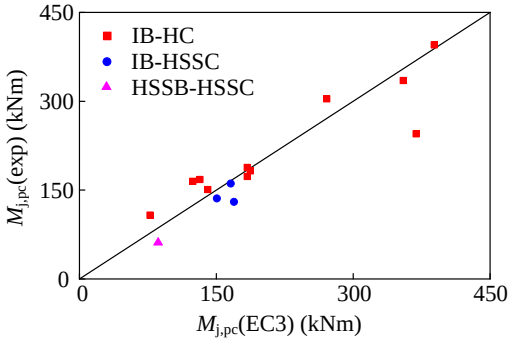

Fig. 14 Comparison of plastic moment obtained from experiments and EC3

not remarkable compared to other configurations, eight blind bolts with a rectangular distributed pattern were still acceptable for the extended end-plate.

4. Analytical method

Table 5 outlines the comparison of moment resistance and initial stiffness between experiments and EC3 regarding three types of beam-to-column joints. Meanwhile, the comparison is diagrammatically depicted in Figs. 13 and 14. It is found that EC3 predicts plastic moment resistance better than initial stiffness for the three types of joints. The initial stiffness of joints with HSS columns was overestimated to some extent compared to those with H-shaped columns. It is noted that the initial stiffness of joints with open-profiled columns can be evaluated appropriately except for those recorded by Coelho *et al.* (2004) as well as Coelho and Bijlaard (2007). The reason explained in the published literature is that the component method in EC3 is limited to the scale of members since the column wall thickness applied in the research approaches up to 40 mm. In order to investigate the moment-rotation relationships, the FE method is a sufficient and economical way of developing a series of models with various characteristics considered. However, it is not a convenient method for the design guidance. An increasing concern is focused on whether a precise analytical model can be proposed to predict the M-ϕ curve. Therefore, a modified component-based method was put forward in this paper to provide an insight into the performance of the steel beam-to-column joints. The flexural behaviour of joints with I-section beams and HSS column has been discussed by Wang *et al.* (2018a), and hence only the joints with HSS beams and HSS columns are analysed.

4.1 Nonlinear model for M-ϕ curve

Based on the literature review (Yee and Melchers 1986), experimental and numerical findings, an M-ϕ curve model

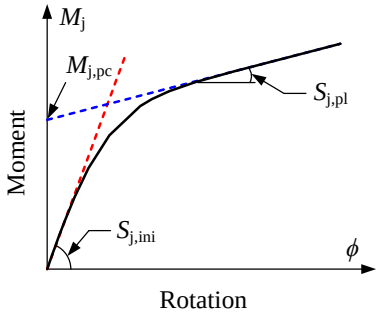

Fig. 15 Typical M-ϕ relationship

adopting three segments was recommended as shown in Fig. 15. The strain hardening was taken into consideration in the model which was ignored by EC3. The model, which had been validated by Ghobarah *et al.* (1996) and Azizinamini *et al.* (1987), demonstrated to be capable of predicting the joint response reasonably well. The corresponding expression was taken as

$$M = M_{j,pc}\left[1-\exp((-S_{j,ini}+S_{j,pl}-C\varphi)\frac{\varphi}{M_{j,pc}})\right] + S_{j,pl}\varphi \quad (4)$$

where C is the rate of decay parameter, ϕ is the joint rotation in radians, $M_{j,pc}$ is the intersection value between the secant of the plasticity and y-axis. Provided that the secant value reduces to 0 which conforms to the assumption of EC3, $M_{j,pc}$ is equal to the moment capacity $M_{j,R}$.

It is noted that the application of the expression relied on several parameters like $S_{j,ini}$, $M_{j,pc}$, $S_{j,pl}$ and C. The first two parameters were determined by an analytical method, while the last two were calibrated based on experimental and numerical results.

By the component method, the initial stiffness and moment capacity can be defined by determining every individual stiffness and capacity respectively and then superimposing the behaviour of each component. In this study, some crucial elements that contributed to the joint behaviour largely were selected for the process based on the parametric analysis mentioned above. The main elements were composed of the end-plate in bending, the column flange in tension and compression, and blind bolts in tension.

4.2 Initial stiffness ($S_{j,ini}$)

According to the basic mechanics theory, the initial stiffness was expressed by

$$S_{j,ini} = \frac{M}{\varphi} \quad (5)$$

The bending moment (M) can be computed by

$$M = F(D_b - t_{bf}) \quad (6)$$

The joint rotation ϕ can be presented based on the deformation compatibility equation by

$$\varphi = \frac{\delta_T}{(D_b - t_{bf})} \quad (7)$$

where δ_T is the total joint deformation, D_b is the beam depth, t_{bf} is the beam flange thickness.

The total joint deformations included those resulting from the end-plate in bending, the column flange in tension and compression, and blind bolts in tension, namely

$$\delta_T = \delta_{ep} + \delta_{cft} + \delta_{cfc} + \delta_{bolt} \quad (8)$$

Substituting Eqs. (6) and (7) into Eq. (5), the initial stiffness can be derived by

$$S_{j,ini} = \frac{F(D_b - t_{bf})^2}{\delta_T} = \frac{F(D_b - t_{bf})^2}{\frac{F}{E}\sum\frac{1}{k_i}} = \frac{E(D_b - t_{bf})^2}{\frac{1}{k_{ep}}+\frac{1}{k_{cft}}+\frac{1}{k_{cfc}}+\frac{1}{k_{bolt}}} \quad (9)$$

It is noted that the individual stiffness is related to the corresponding deformations which have been determined by Wang *et al.* (2018a).

As for the end-plate in bending, the deflection can be given by

$$\delta_{ep}(x,y) = \frac{4F}{\pi^6 D|x_2 - x_1||y_2 - y_1|} \times\sum_{m=1}^{\infty}\sum_{n=1}^{\infty}\frac{\left(\cos\frac{m\pi x_{ep1}}{a_{ep}} - \cos\frac{m\pi x_{ep2}}{a_{ep}}\right)}{mn\left(\frac{m^2}{a_{ep}^2}+\frac{n^2}{b_{ep}^2}\right)^2} \times\left(\cos\frac{n\pi y_{ep1}}{b_{ep}} - \cos\frac{n\pi y_{ep2}}{b_{ep}}\right) \times\left(\sin\frac{m\pi x}{a_{ep}}\sin\frac{n\pi y}{b_{ep}}\right) \quad (10)$$

where a_{ep} and b_{ep} represent the horizontal and vertical spacing between bolts respectively, (x_{ep1}, y_{ep1}), (x_{ep2}, y_{ep2}) are diagonal points of a distributed load area, D is the flexural rigidity which equals to $Et^3/(12(1\text{-}\nu^2))$.

The deflections of the column flange in tension can be derived by

$$\delta_{cft}(x,y) = \frac{4F_{RB}}{\pi^4 a_{cft} b_{cft} D}\sum_{m=1}^{\infty}\sum_{n=1}^{\infty}\frac{\sin\frac{m\pi\xi}{a_{cft}}\sin\frac{n\pi\eta}{b_{cft}}}{\left(\frac{m^2}{a_{cft}^2}+\frac{n^2}{b_{cft}^2}\right)^2} \times\left(\sin\frac{m\pi x}{a_{cft}}\sin\frac{n\pi y}{b_{cft}}\right) \quad (11)$$

$$F_{\mathrm{RB}}(x,y)=2D(1-\nu)\left(\frac{\partial^2\delta_{\mathrm{ep}}}{\partial x\partial y}\right)$$
$$=\frac{8F(1-\nu)}{\pi^4 a_{\mathrm{ep}}b_{\mathrm{ep}}\left|x_{\mathrm{ep2}}-x_{\mathrm{ep1}}\right|\left|y_{\mathrm{ep2}}-y_{\mathrm{ep1}}\right|}$$
$$\times\sum_{m=1}^{\infty}\sum_{n=1}^{\infty}\frac{\left(\cos\frac{m\pi x_{\mathrm{ep1}}}{a_{\mathrm{ep}}}-\cos\frac{m\pi x_{\mathrm{ep2}}}{a_{\mathrm{ep}}}\right)}{\left(\frac{m^2}{a_{\mathrm{ep}}{}^2}+\frac{n^2}{b_{\mathrm{ep}}{}^2}\right)^2} \qquad (12)$$
$$\times\left(\cos\frac{n\pi y_{\mathrm{ep1}}}{b_{\mathrm{ep}}}-\cos\frac{n\pi y_{\mathrm{ep2}}}{b_{\mathrm{ep}}}\right)$$
$$\times\left(\cos\frac{m\pi x}{a_{\mathrm{ep}}}\cos\frac{n\pi y}{b_{\mathrm{ep}}}\right)$$

where a_{cft} denotes a clear width of the column flange which is equal to (B_{c}-2t_{c}), b_{cft} is taken as a distance between the neutral axis of the beam and the edge of end-plate, (ξ, η) is the location of point loads (F_{RB}).

The column flange in compression deformed due to a pressure resulting from the beam flange in compression, and its deflections were expressed by Eq. (10). An effective region of the local distributed load was denoted as

$$\left|x_2-x_1\right|=B_{\mathrm{bf}}+2(t_{\mathrm{w}}+t_{\mathrm{ep}}+t_{\mathrm{c}}) \qquad (13)$$

$$\left|y_2-y_1\right|=t_{\mathrm{bf}}+2(t_{\mathrm{w}}+t_{\mathrm{ep}}+t_{\mathrm{c}}) \qquad (14)$$

where B_{bf} is the width of beam flanges; t_{w} is the size of fillet welds.

Elongations of bolt shanks can be determined by

$$\delta_{\mathrm{bolt}}=\frac{F_{\mathrm{RB}}L_{\mathrm{bt}}}{E_{\mathrm{bt}}A_{\mathrm{bt}}} \qquad (15)$$

where L_{bt} is the length of bolt shanks between bolt heads and nuts, E_{bt} is the Young's Modulus of blind bolts, A_{bt} is the tensile stress area of bolt shanks.

4.3 Moment capacity ($M_{\mathrm{j,pc}}$)

The moment resistance $M_{\mathrm{j,pc}}$ depended on the strength of the individual components. Considerable investigations indicated that the resistance can be reflected by one (or more) of the following failure modes:

(i) Bolt failure (in tension)
(ii) End-plate failure
(iii) Column flange failure

As for each failure mode, the corresponding force (F_{f}) on the beam flanges in tension and compression can be determined. Substituting the lowest value of F_{f} into Eq. (6), the expression for the moment capacity can be revised by

$$M_{\mathrm{j,pc}}=F_{\mathrm{f}}(D_{\mathrm{b}}-t_{\mathrm{bf}}) \qquad (16)$$

4.3.1 Bolt failure

Since the joint performance with double bolt-rows in tension was stronger than that with single bolt-row in tension, only the former configuration was considered herein. The maximum force $F_{\mathrm{f(bt)}}$ was then given by

$$F_{\mathrm{f(bt)}}=\chi_{\mathrm{b}}N_{\mathrm{b}}f_{\mathrm{ybt}}A_{\mathrm{bt}} \qquad (17)$$

where χ_{b} is the bolt force prying factor. Yee and Melchers (1986) suggested the value should be taken as 0.75, N_{b} is the total number of bolts in tension and f_{ybt} is the yield stress of bolts.

4.3.2 End-plate failure

Ghobarah *et al*. (1996) improved the Walpole (1985) formula by considering a reduction effect of the bending stiffness due to the presence of high strength bolt holes. Two different yield line mechanisms can be presented by

$$F_{\mathrm{f(ep)}}=f_{\mathrm{yep}}t_{\mathrm{ep}}{}^2\left[\frac{2(B_{\mathrm{ep}}-d_{\mathrm{b}})}{Y_{\mathrm{b}}-t_{\mathrm{bf}}-2t_{\mathrm{w}}}+\frac{2(p-d_{\mathrm{b}}/2)}{(X_{\mathrm{b}}-t_{\mathrm{bw}}-2t_{\mathrm{w}})}\right] \qquad (18)$$

$$F_{\mathrm{f(ep)}}=\frac{f_{\mathrm{yep}}t_{\mathrm{ep}}{}^2(B_{\mathrm{ep}}-d_{\mathrm{b}})}{h} \qquad (19)$$

where f_{yep} is the yield stress of end-plates, B_{ep} is the width of end-plates, X_{b} and Y_{b} are the horizontal and vertical spacing between bolts respectively, t_{bf} and t_{bw} are the thickness of the beam flange and beam web respectively, h is the distance from one bolt-row to the centre of fillet welds, p = 0.6(d_{b}-t_{bf}).

4.3.3 Column flange failure

Meanwhile, Ghobarah *et al*. (1996) proposed two possible failure modes of column flanges on the tension side of joints. The corresponding loads were given by

$$F_{\mathrm{f(cft)}}=\frac{2f_{\mathrm{yc}}t_{\mathrm{c}}{}^2}{(1\text{-}\alpha)}\left[(\beta-\gamma)+2\sqrt{(1-\gamma)(1-\alpha)}\right] \qquad (20)$$

$$F_{\mathrm{f(cft)}}=f_{\mathrm{yc}}t_{\mathrm{c}}{}^2\left[\pi\left(1-\frac{\gamma}{2(1-\alpha)}+2\frac{(\alpha+\beta-\gamma)}{(1-\alpha)}\right)\right] \qquad (21)$$

where f_{yc} is the yield stress of tubes, α, β and γ are taken as

$$\alpha=\frac{X_{\mathrm{b}}}{(B_{\mathrm{c}}\text{-}t_{\mathrm{c}})},\qquad \beta=\frac{Y_{\mathrm{b}}}{(B_{\mathrm{c}}\text{-}t_{\mathrm{c}})},\qquad \gamma=\frac{D_{\mathrm{b}}}{(B_{\mathrm{c}}\text{-}t_{\mathrm{c}})} \qquad (22)$$

4.4 Evaluation of strain-hardening stiffness ($S_{\mathrm{j,pl}}$) and parameter C

Theoretically, the strain-hardening stiffness is the secant value of the moment-rotation curve at the plastic stage. It can intuitively reflect the plastic response of the beam-to-column joint. The numerical results summarised in Table 6 indicated that there exist correlations between the initial stiffness and strain-hardening stiffness. The ratio of strain

Table 6 Comparison of moment resistance and stiffness between numerical and analytical results

	Numerical values					Analytical values					
	$M_{j,E}$ (kNm)	$M_{j,R}$ (kNm)	$S_{j,ini}$ (kNm/rad)	$S_{j,pl}$ (kNm/rad)	$S_{j,pl}$/ $S_{j,ini}$ (%)	$M_{j,R}$ (kNm)	Error (%)	$S_{j,ini}$ (kNm/rad)	Error (%)	$S_{j,pl}$ (kNm/rad)	Error (%)
f_y = 300	43	96	3527	367	10	95	0	3796	8	380	4
f_y = 340	45	100	3648	368	10	101	1	3796	4	380	3
f_y = 360	46	104	3654	337	9	107	3	3796	4	380	13
t_{ep} = 8	31	71	2515	293	12	58	-18	2456	-2	246	-16
t_{ep} = 10	37	82	3056	327	11	83	1	3237	6	324	-1
t_{ep} = 16	60	119	4917	399	8	116	-3	4484	-9	448	12
t_b = 6	41	92	3322	352	11	94	2	3718	12	372	6
t_b = 12.5	47	96	3854	368	10	93	-3	3760	-2	376	2
t_c = 16	56	106	4625	484	11	112	6	5505	19	551	14
d_b = 20	44	96	3622	378	10	95	-1	3796	5	380	1
d_b = 24	46	100	3763	418	11	93	-7	3796	1	380	-9
SBRT-1	30	55	2346	210	9	-	-	-	-	-	-
SBRT-2	33	62	2844	203	7	-	-	-	-	-	-
SBRT-3	20	83	1619	139	9	-	-	-	-	-	-
SBRT-4	40	87	3232	361	11	-	-	-	-	-	-
DBRT-1	38	88	2943	310	11	87	-1	3170	8	317	2
DBRT-2	44	100	3580	378	11	94	-6	3650	2	365	-3
DBRT-3	46	103	3737	417	11	96	-7	3796	2	380	-9

hardening stiffness to initial stiffness was observed to be around 9% to 11%. Since the analytical model was to be used in evaluating the joint performance with double bolt-rows in tension, it was believed that small variations of the strain-hardening stiffness cannot influence the joint response significantly. In order to simplify and unify the proposed model as much as possible, the strain-hardening stiffness in this study was taken as 10% of the initial stiffness.

The parameter C controlled the rate of decay of moment-rotation curves. As noted in Eq. (4), the initial slope was associated with the value. When the parameter C was approaching infinity, the moment-rotation relationship of the joint appeared to exhibit the bilinear behaviour with the yield moment being equal to $M_{j,pc}$. In general, the value of C depended on experimental results as well as empirical research. Ghobarah *et al*. (1996) recommended the value to be 10^5 kN·m/rad^2, which was appropriate for joints with HSS columns.

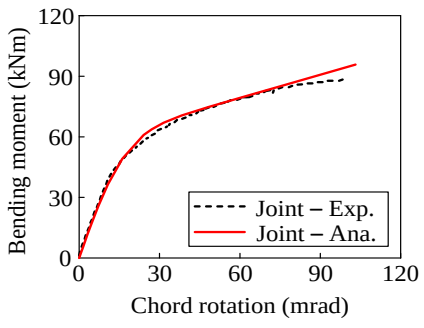

Fig. 16 Comparison between experimental results and analytical model

4.5 Model validation and discussion

The moment-rotation curve of the joint has been solved based on the analytical model mentioned above, which was compared to experimental results shown in Fig. 16. In the meantime, a comparison between analytical models and FE models is summarised in Table 6, including the moment capacity ($M_{j,R}$), the initial stiffness ($S_{j,ini}$) and the strain-hardening stiffness ($S_{j,pl}$). Since the beam-to-column joints with single bolt-row in tension were not recommended, they were neglected in this section.

It can be seen from Fig. 16 that the proposed analytical model predicted the test results reasonably well. Furthermore, the highlight was that there was an adequate predicting accuracy at the elastic stage and strain-hardening stage. As indicated in Table 6, the discrepancy between FE models and analytical models was small. Overall, the validation demonstrated that the analytical model was capable of providing satisfactory solutions for the beam-to-column joints.

It is also noted that the individual deformations in Eqs. (10)-(12) were determined by numerous iteration cycles achieving highly accurate results. To simplify the computation and obtain individual stiffness conveniently, the sensitivity of iteration cycles was compared as indicated in Fig. 17, where the initial stiffness was computed based on five kinds of cycles. The results evidently suggested that the analytical results remained appropriately precise when the iteration reduced to one cycle. Accordingly, Eqs. (1)-

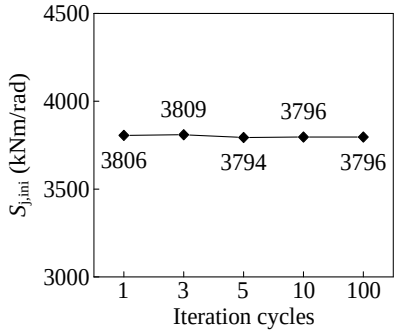

Fig. 17 Iteration cycle sensitivity analytical results

(12) can be further simplified to obtain various component deformations.

$$\delta_{ep}=\frac{4F}{\pi^6 D\left|x_{ep2}-x_{ep1}\right|\left|y_{ep2}-y_{ep1}\right|}\times\frac{\left(\cos\frac{\pi x_{ep1}}{a_{ep}}-\cos\frac{\pi x_{ep2}}{a_{ep}}\right)}{\left(\frac{1}{a_{ep}^{\ 2}}+\frac{1}{b_{ep}^{\ 2}}\right)^2}\times\left(\cos\frac{\pi y_{ep1}}{b_{ep}}-\cos\frac{\pi y_{ep2}}{b_{ep}}\right) \tag{23}$$

$$\delta_{cft}=\frac{16F_{RB}}{\pi^4 a_{cft}b_{cft}D}\times\frac{\sin\frac{\pi\xi}{a_{cft}}\sin\frac{\pi\eta}{b_{cft}}}{\left(\frac{1}{a_{cft}^{\ 2}}+\frac{1}{b_{cft}^{\ 2}}\right)^2} \tag{24}$$

$$F_{RB}=\frac{8F(1-\nu)}{\pi^4 a_{ep}b_{ep}\left|x_{ep2}-x_{ep1}\right|\left|y_{ep2}-y_{ep1}\right|}\times\frac{\left(\cos\frac{\pi x_{ep1}}{a_{ep}}-\cos\frac{\pi x_{ep2}}{a_{ep}}\right)}{\left(\frac{1}{a_{ep}^{\ 2}}+\frac{1}{b_{ep}^{\ 2}}\right)^2}\times\left(\cos\frac{\pi y_{ep1}}{b_{ep}}-\cos\frac{\pi y_{ep2}}{b_{ep}}\right) \tag{25}$$

5. Design recommendations

The analytical method mentioned above provided a reliable approach to predict the moment-rotation performance of steel beam-to-column joints with hollow sections. In particular, the estimation of initial stiffness incorporating double bolt-rows in tension was superior to EC3. As a result, the modified component method was recommended for the design of HSS beam to HSS column joints.

Four stiffness coefficients were considered to define the effective stiffness coefficient, including the end-plate in bending, column wall in tension, column wall in compression and blind bolts in tension. The expressions can be denoted as

End-plate in bending

$$k_{ep}=\frac{\pi^6 t_{ep}^{\ 3}}{48(1-\nu^2)}\times\frac{\left|x_{ep2}-x_{ep1}\right|\left|y_{ep2}-y_{ep1}\right|}{\left(\cos\frac{\pi x_{ep1}}{a_{ep}}-\cos\frac{\pi x_{ep2}}{a_{ep}}\right)}\times\frac{\left(\frac{1}{a_{ep}^{\ 2}}+\frac{1}{b_{ep}^{\ 2}}\right)^2}{\left(\cos\frac{\pi y_{ep1}}{b_{ep}}-\cos\frac{\pi y_{ep2}}{b_{ep}}\right)} \tag{26}$$

Column wall in tension

$$k_{cft}=\frac{\pi^4 a_{cft}b_{cft}t_c^{\ 3}}{192(1-\nu^2)}\frac{F}{F_{RB}}\times\frac{\left(\frac{1}{a_{cft}^{\ 2}}+\frac{1}{b_{cft}^{\ 2}}\right)^2}{\sin\frac{\pi\xi}{a_{cft}}\sin\frac{\pi\eta}{b_{cft}}} \tag{27}$$

$$\frac{F}{F_{RB}}=\frac{\pi^4 a_{ep}b_{ep}}{8(1-\nu)}\times\frac{\left|x_{ep2}-x_{ep1}\right|\left|y_{ep2}-y_{ep1}\right|}{\left(\cos\frac{\pi x_{ep1}}{a_{ep}}-\cos\frac{\pi x_{ep2}}{a_{ep}}\right)}\times\frac{\left(\frac{1}{a_{ep}^{\ 2}}+\frac{1}{b_{ep}^{\ 2}}\right)^2}{\left(\cos\frac{\pi y_{ep1}}{b_{ep}}-\cos\frac{\pi y_{ep2}}{b_{ep}}\right)} \tag{28}$$

Column wall in compression

$$k_{cfc}=\frac{\pi^6(\lambda t_c)}{48(1-\nu^2)}\times\frac{\left|x_{cfc2}-x_{cfc1}\right|\left|y_{cfc2}-y_{cfc1}\right|}{\left(\cos\frac{\pi x_{cfc1}}{a_{cfc}}-\cos\frac{\pi x_{cfc2}}{a_{cfc}}\right)}\times\frac{\left(\frac{1}{a_{cfc}^{\ 2}}+\frac{1}{b_{cfc}^{\ 2}}\right)^2}{\left(\cos\frac{\pi y_{cfc1}}{b_{cfc}}-\cos\frac{\pi y_{cfc2}}{b_{cfc}}\right)} \tag{29}$$

Blind bolts in tension

$$k_{\text{bolt}} = \frac{A_{\text{bt}}}{L_{\text{bt}}} \frac{F}{F_{\text{RB}}} \tag{30}$$

Moment resistance was suggested to refer to Section 4.3 with the aim of achieving moment-rotation curves that were consistent with experiments.

6. Conclusions

The moment-rotation response of steel beam-to-column sub-assemblages, including HSS beams, HSS columns, extended end-plates and blind bolts, has been investigated in this paper. The investigation was mainly based on the FE analysis which has been validated by the experimental results and compared to EC3. In particular, the feasibility analysis of the structural demountability has been highlighted. The specific parametric study has been performed aiming to evaluate the factors that influenced the joints behaviour significantly. Finally, an analytical model was proposed to provide more accurate predictions and design recommendations. Some key conclusions can be drawn as follows:

- By investigating the moment-strain behaviour of some critical components, the loading capacity of the semi-rigid joint achieving the demountability accounts for about 53% of the ultimate capacity, which is larger than the typical service load. It is feasible for steel components under the serviceability limited state to be dismantled and reused at the end of a service life. In addition, the current design approach in EC3 overestimates the initial stiffness extensively.
- The validated FE model is able to predict the flexural behaviour of the steel beam-to-column joints in terms of the initial stiffness and moment capacity. A total of six parameters are considered to assess the effect on the joint performance. The end-plate thickness and the column wall thickness are the two most crucial factors that have significant influences on the structural response. In addition, the bolted connection layout, double bolt-rows in tension, is recommended for the beam-to-column joints when the extended end-plates are involved.
- The moment-rotation curve is estimated by deriving formulations of initial stiffness and moment resistance. The proposed analytical model, which has been validated by the experimental and numerical results, predicts moment-resisting performance of steel beam-to-column joints reasonably well. The method can be applied to the joint behaviour with double bolt-rows in tension.
- The individual stiffness coefficients of critical components are derived based on the modified component method. The simplified approach is recommended for HSS beam to HSS column joints with extended end-plates, and it is fairly reliable to be utilised to provide design guidance for the joints in future.

Acknowledgments

The research described in this paper is financially supported by the Australian Research Council (ARC) under its Discovery Scheme (Project No: DP140102134). The financial support is gratefully acknowledged. Acknowledgement is also made to the staff in the Heavy Structures Laboratory at the University of New South Wales for assisting with the experimental testing.

References

Abaqus (2014), User Manual; Version 6.14, DS SIMULIA Corp., Providence, RI, USA.

AS/NZS 1252.1 (2016), High-strength steel fastener assemblies for structural engineering—Bolts, nuts and washers, Australia.

AS 1391 (2007), Australian. Metallic materials—tensile testing at ambient temperature, Australia.

AS 4100 (1998), Steel structures, Australia.

Augusto, H., da Silva, L.S., Rebelo, C. and Castro, J.M. (2016a), "Characterization of web panel components in double-extended bolted end-plate steel joints", *J. Constr. Steel Res.*, **116**, 271-293.

Augusto, H., Castro, J.M., Rebelo, C. and da Silva, L.S. (2016b), "Characterization of the cyclic behavior of the web components in end-plate beam-to-column joints", *Procedia Eng.*, **160**, 101-108.

Azizinamini, A., Bradburn, J.H. and Radziminski, J.B. (1987), "Initial stiffness of semi-rigid steel beam-to-column connections", *J. Constr. Steel Res.*, **8**, 71-90.

Coelho, A.M.G. and Bijlaard, F.S. (2007), "Experimental behaviour of high strength steel end-plate connections", *J. Constr. Steel Res.*, **63**(9), 1228-1240.

Coelho, A.M.G., Bijlaard, F.S. and da Silva, L.S. (2004), "Experimental assessment of the ductility of extended end plate connections", *Eng. Struct.*, **26**(9), 1185-1206.

da Silva, L.S., de Lima, L.R., da SVellasco, P.C.G. and de Andrade, S.A. (2004), "Behaviour of flush end-plate beam-to-column joints under bending and axial force", *Steel Compos. Struct., Int. J.*, **4**(2), 77-94.

EN1993-1-8 (2005), Eurocode 3: Design of steel structures. part 1-8: design of joints; European Committee for Standardization, Brussels, Belgium.

France, J.E., Davison, J.B. and Kirby, P.A. (1999), "Strength and rotational stiffness of simple connections to tubular columns using flowdrill connectors", *J. Constr. Steel Res.*, **50**(1), 15-34.

Ghobarah, A., Mourad, S. and Korol, R.M. (1996), "Moment-rotation relationship of blind bolted connections for HSS columns", *J. Constr. Steel Res.*, **40**(1), 63-91.

Grimsmo, E.L., Clausen, A.H., Langseth, M. and Aalberg, A. (2015), "An experimental study of static and dynamic behaviour of bolted end-plate joints of steel", *Int. J. Impact Eng.*, **85**, 132-145.

Han, L.H., Wang, W.D. and Zhao, X.L. (2008), "Behaviour of steel beam to concrete-filled SHS column frames: Finite element model and verifications", *Eng. Struct.*, **30**(6), 1647-1658.

Korol, R.M., Ghobarah, A. and Mourad, S. (1993), "Blind bolting W-shape beams to HSS columns", *J. Struct. Eng.*, **119**(12), 3463-3481.

Li, D., Uy, B., Aslani, F. and Patel, V. (2016a), "Analysis and design of demountable steel column-baseplate connections", *Steel Compos. Struct., Int. J.*, **22**(4), 753-775.

Li, D., Uy, B., Patel, V. and Aslani, F. (2016b), "Behaviour and design of demountable steel column-column connections", *Steel*

Compos. Struct., Int. J., **22**(2), 429-448.
Loh, H.Y., Uy, B. and Bradford, M.A. (2006), "The effects of partial shear connection in composite flush end plate joints Part I—experimental study", *J. Constr. Steel Res.*, **62**(4), 378-390.
Mirza, O. and Uy, B. (2011), "Behaviour of composite beam–column flush end-plate connections subjected to low-probability, high-consequence loading", *Eng. Struct.*, **33**(2), 647-662.
Nogueiro, P., da Silva, L.S., Bento, R. and Simões, R. (2009), "Calibration of model parameters for the cyclic response of end-plate beam-to-column steel-concrete composite joints", *Steel Compos. Struct., Int. J.*, **9**(1), 39-58.
Odrobiňák, J., Idunk, R. and Bačinský, T. (2014), "Study on Stiffness of Composite Beam-to-Column Joints", *Procedia Eng.*, **91**, 268-273.
Petrina, T. (2016), "Fire Resistance of Steel Beam to Column End Plate Connections", *Procedia Eng.*, **161**, 143-149.
Qiang, X., Bijlaard, F.S.K., Kolstein, H. and Jiang, X. (2014), "Behaviour of beam-to-column high strength steel endplate connections under fire conditions–Part 1: Experimental study", *Eng. Struct.*, **64**, 23-38.
Rehman, N., Lam, D., Dai, X. and Ashour, A.F. (2016), "Experimental study on demountable shear connectors in composite slabs with profiled decking", *J. Constr. Steel Res.*, **122**, 178-189.
Sun, R., Burgess, I.W., Huang, Z. and Dong, G. (2015), "Progressive failure modelling and ductility demand of steel beam-to-column connections in fire", *Eng. Struct.*, **89**, 66-78.
Thai, H.T., Vo, T.P., Nguyen, T.K. and Pham, C.H. (2017), "Explicit simulation of bolted endplate composite beam-to-CFST column connections", *Thin-Wall. Struct.*, **119**, 749-759.
Uy, B., Patel, V., Li, D.X. and Aslani, F. (2017), "Behaviour and design of connections for demountable steel and composite structures", *Structures*, **9**, 1-12.
Walpole, W.R. (1985), "Beam-column joints", *Bull. New Zealand Nat. Soc. Earthq. Eng.*, **18**, 369-379.
Wang, J., Uy, B. and Li, D. (2018a), "Analysis of demountable steel and composite frames with semi-rigid bolted joints", *Steel Compos. Struct., Int. J.*, **28**(3), 363-380.
Wang, J., Uy, B., Thai, H.T. and Li, D. (2018b), "Behaviour and design of demountable beam-to-column composite bolted joints with extended end-plates", *J. Constr. Steel Res.*, **144**, 221-235.
Yee, Y.L. and Melchers, R.E. (1986), "Moment-rotation curves for bolted connections", *J. Struct Eng.*, **112**(3), 615-635.

DL

Notation

A_{bt} Tensile stress area of bolt

A_{mn} Coefficient of the deformations equation for a simply-supported thin plate.

B_{bf} Width of beam flange

B_c Width of column wall

B_{ep} Width of end-plate

C Rate of decay parameter

D Flexural rigidity (equals to $Et^3/(12(1-v^2))$)

D_b Beam depth

E Young's Modulus

F Load of couple applied on beam flanges

F_f Load of couple resulting in component failure

$F_{f(bt)}$ Load of couple resulting in bolt failure

$F_{f(ep)}$ Load of couple resulting in end-plate failure

$F_{f(cft)}$ Load of couple resulting in column flange failure

F_{RB} Reaction of four corners of thin plate

I_b Second moment of area of beam

L_b Span of beam

L_{load} Distance between loading point and end-plate

M Bending moment

$M_{j,E}$ Maximum elastic bending moment before approaching plastic response

$M_{j,pc}$ Plastic bending moment that one component fails

$M_{j,R}$ Moment capacity of structure

N_b Amount of bolts in tension

P Load applied on beam

$S_{j,ini}$ Initial stiffness

$S_{j,pl}$ Strain-hardening stiffness

X_b Horizontal space between bolts

Y_b Vertical space between bolts

a and b Length and width of thin plate

d_b Bolt diameter

f_y Steel yield strength

f_{ybt} Yield strength of bolt

f_{yc} Yield strength of column

f_{yep} Yield strength of end-plate

h Distance from one bolt-row to centre of fillet weld

k_{bolt} Stiffness coefficient of blind bolt in tension

k_{cfc} Stiffness coefficient of column flange in compression

k_{cft} Stiffness coefficient of column flange in tension

k_{ep} Stiffness coefficient of end-plate

m and n Positive integers

q Distributed loads applied vertically to thin plate

t_b Beam thickness

t_{bf} Beam flange thickness

t_{bw} Beam web thickness

t_c Column wall thickness

t_{ep} End-plate thickness

t_w Size of fillet weld

α Ratio of relative horizontal bolt spacing to (B_c-t_c)

β Ratio of relative vertical bolt spacing to (B_c-t_c)

γ Ration of relative beam depth to (B_c-t_c)

δ_{bolt} Deformations of blind bolt in tension

δ_{cfc} Deformations of column flange in compression

δ_{cft} Deformations of column flange in tension

δ_{ep} Deformations of end-plate

δ_{LVDT} Vertical deformations at bottom end of column

δ_T Total deformations resulting from column flange in compression, column flange in tension and end-plate

λ Amplification factor

v Poisson's ratio

χ_b Bolt force prying factor

ϕ Rotational deformations of joint

ϕ_{ep} Rotational deformations of end-plate

ϕ_s Shear deformations of column web panel zone

$\phi_{Mj,E}$ Rotational deformations corresponding to $M_{j,E}$

$\phi_{Mj,R}$ Rotational deformations corresponding to $M_{j,R}$